Article

Satellite-Based Evaluation of Submarine Permafrost Erosion at Shallow Offshore Areas in the Laptev Sea

Alexander Osadchiev [1,2,3,*], Polina Adamovskaya [4], Stanislav Myslenkov [5], Oleg Dudarev [3,6] and Igor Semiletov [3,6]

[1] Shirshov Institute of Oceanology, Russian Academy of Sciences, Nahimovskiy Prospect 36, Moscow 117997, Russia
[2] Moscow Institute of Physics and Technology, Institusky Lane 9, Dolgoprudny 141701, Russia
[3] National Research Tomsk State University, Lenin Avenue 36, Tomsk 634050, Russia; dudarev@poi.dvo.ru (O.D.); ipsemiletov@gmail.com (I.S.)
[4] Russian State Hydrometeorological University, Malookhtinskiy Prospekt 98, St. Petersburg 195196, Russia; polina.adamovskaya@gmail.com
[5] Department of Oceanology, Faculty of Geography, Lomonosov Moscow State University, Leninskie Gory 1, Moscow 119991, Russia; myslenkov@nral.org
[6] Ilyichev Pacific Oceanological Institute, Far Eastern Branch of the Russian Academy of Sciences, Baltiyskaya Street 43, Vladivostok 690041, Russia
* Correspondence: osadchiev@ocean.ru

Abstract: Large areas of the seafloor in the Laptev Sea consist of submarine permafrost, which has experienced intense degradation over the last decades and centuries. Thermal abrasion of the submarine permafrost results in upward advection of suspended matter, which could reach the surface layer in shallow areas. This process is visually manifested through increased turbidity of the sea surface layer, which is regularly detected in optical satellite imagery of the study areas. In this study, satellite data, wind and wave reanalysis, as well as in situ measurements are analyzed in order to reveal the main mechanisms of seafloor erosion in shallow areas of the Laptev Sea. We describe the synoptic variability in erosion at the Vasilyevskaya and Semenovskaya shoals in response to wind and wave conditions. Finally, using reanalysis data, daily suspended matter flux from this area was evaluated during ice-free periods in 1979–2021, and its seasonal and inter-annual variabilities were described. The obtained results contribute to our understanding of subsea permafrost degradation, the sediment budget, and carbon and nutrient cycles in the Laptev Sea.

Keywords: bottom sediments; coastal upwelling; seafloor erosion; submarine permafrost; thermal abrasion; suspended matter flux; wind and wave forcing; Laptev Sea; Arctic Ocean

1. Introduction

The Arctic Ocean is extremely vulnerable to the ongoing climate change. In general, warming of the Arctic is evident through a reduction in ice coverage and increase in air temperatures [1,2]. In certain areas, it also results in intense coastal retreat [3–6] and degradation of subsea permafrost [7–9]. The latter processes are especially important in the Laptev Sea, which is characterized by wide coastal and submarine permafrost areas [10–14]. Coastal and submarine permafrost in the Laptev Sea is a large carbon pool degradation, which is directly related to greenhouse gas emissions [4,15,16]. Moreover, oxidation of eroded carbon to carbon dioxide (CO_2) plays a primary role in supersaturation of the water column in the Laptev Sea and the adjacent part of the East Siberian Sea, and causes extreme acidification there [17–19].

Thawing of the Arctic permafrost could release significant amounts of carbon into the atmosphere in this century. Ancient ice complex deposits outcrop along the ~7000 km coastline of the East Siberian Arctic shelf and the associated shallow subsea permafrost are two large pools of permafrost carbon, yet their vulnerabilities towards thawing and

decomposition are largely unknown [15,20]. Recent Arctic warming has been stronger than was predicted by several degrees, and has been particularly pronounced over the coastal East Siberian Arctic. Increasing Lena River heat discharge and wind-induced water mixing causes progressive warming of the surface sediments and high rates of vertical subsea permafrost degradation [7,21]. There is, thus, a pressing need to improve our understanding of the links between permafrost carbon and climate change in this low-accessible region.

Coastal erosion and river discharge are the main sources of suspended sediment in the Laptev Sea, which were explicitly studied in previous works [22–24]. Horizontal and vertical transport of suspended matter within the sea is governed by the spreading and mixing of large river plumes, as well as coastal and shelf currents, which have large seasonal and inter-annual variability [25–33]. Entrainment of suspended matter by sea ice and its subsequent advection to the deep central part of the Arctic Ocean during the cold season is an important mechanism of the large-scale export of suspended sediments from the Laptev Sea [27,34–36].

Seafloor erosion could also contribute to the sediment budget of the Laptev Sea. Generally, this process occurs in shallow areas where wind and wave turbulence from the surface layer reaches the seafloor and causes the entrainment of bottom sediments to the water column [15,37–39]. In the Arctic Ocean, erosion of subsea permafrost areas is also affected by the temperature of the sea bottom layer [40]. In certain shallow areas, eroded sediments could rise up to the surface layer and significantly increase its turbidity. In particular, intense seafloor erosion in different parts of the Laptev Sea often manifests in satellite imagery through the appearance of turbid sea areas [41,42]. However, this process has received little attention before. In particular, we are not aware of any comprehensive study that addressed the dynamics of and variability in seafloor erosion in shallow areas in the Laptev Sea and provided the related assessments of sediment fluxes.

This paper is focused on seafloor erosion in several of the largest shoals in the Laptev Sea, where this process is detected by satellite observations. The general scheme of the suggested methodology is the following. First, we calculate the area (in km^2) of turbid zones (formed as a result of seafloor erosion at the shoals) visible in optical satellite imagery. As a result, we obtain information about the intensity of seafloor erosion, albeit only during ~100 cloud-free and ice-free days during 2000–2021 due to satellite data temporal coverage. We compare the calculated areas of turbid zones with synchronous wind-wave conditions, reconstructed for the considered days using the numerical model. After we obtain the dependence of the intensity of seafloor erosion on wind-wave conditions, we reconstruct this intensity for every ice-free day during 1979–2021 due to numerical model temporal coverage. Finally, we use these data and in situ measurements of sediment concentrations to assess the eroded sediment matter flux from this shoal during the ice-free seasons in 1979–2021.

The following paper is structured in the following way. Section 2 describes the study area, as well as the satellite, wind and wave reanalysis, and the in situ data used in this work. The results from the processing of the satellite data and a description of the spatial and temporal variability in turbid erosion-induced areas pertain to Section 3. In Section 4, the numerical dependences between the intensity of seafloor erosion and wind-wave forcing is described. Based on this result, the flux of eroded sediments and its seasonal and inter-annual variability scales are evaluated and discussed. The conclusions are then presented in Section 5.

2. Data and Methods

2.1. Study Area

The Laptev Sea is a marginal sea of the Arctic Ocean located off the northeastern coast of Siberia (Figure 1). This sea is bounded by the Taimyr Peninsula and the Severnaya Zemlya archipelago in the west and the New Siberian Islands in the east. Compared to the western and eastern regions of the Eurasian Arctic influenced by cyclonic activity of the Atlantic and Pacific oceans, respectively, the Laptev Sea has severe climate conditions

including extremely low winter temperatures and a short ice-free season [43]. Intense ice melting starts in late June–early July, and by August–September the whole sea is free of ice. Ice formation starts in October, and by late October–early November the Laptev Sea is completely covered by ice [30]. The Laptev Sea is shallow, and half of the sea area is located at the continental shelf with depths < 50 m.

According to recent thermodynamic sediment data and electromagnetic surveys, the submarine permafrost is continuous for the major part of the Laptev Sea shelf from the shoreline up to isobaths of 80–100 m [44,45]. However, at certain shelf areas, the submarine permafrost is discontinuous and contains gas and gas hydrate accumulations. The submarine permafrost layer has a thickness of several hundred meters, which degrades at a rate of about 14–18 cm per year [7,11,46,47].
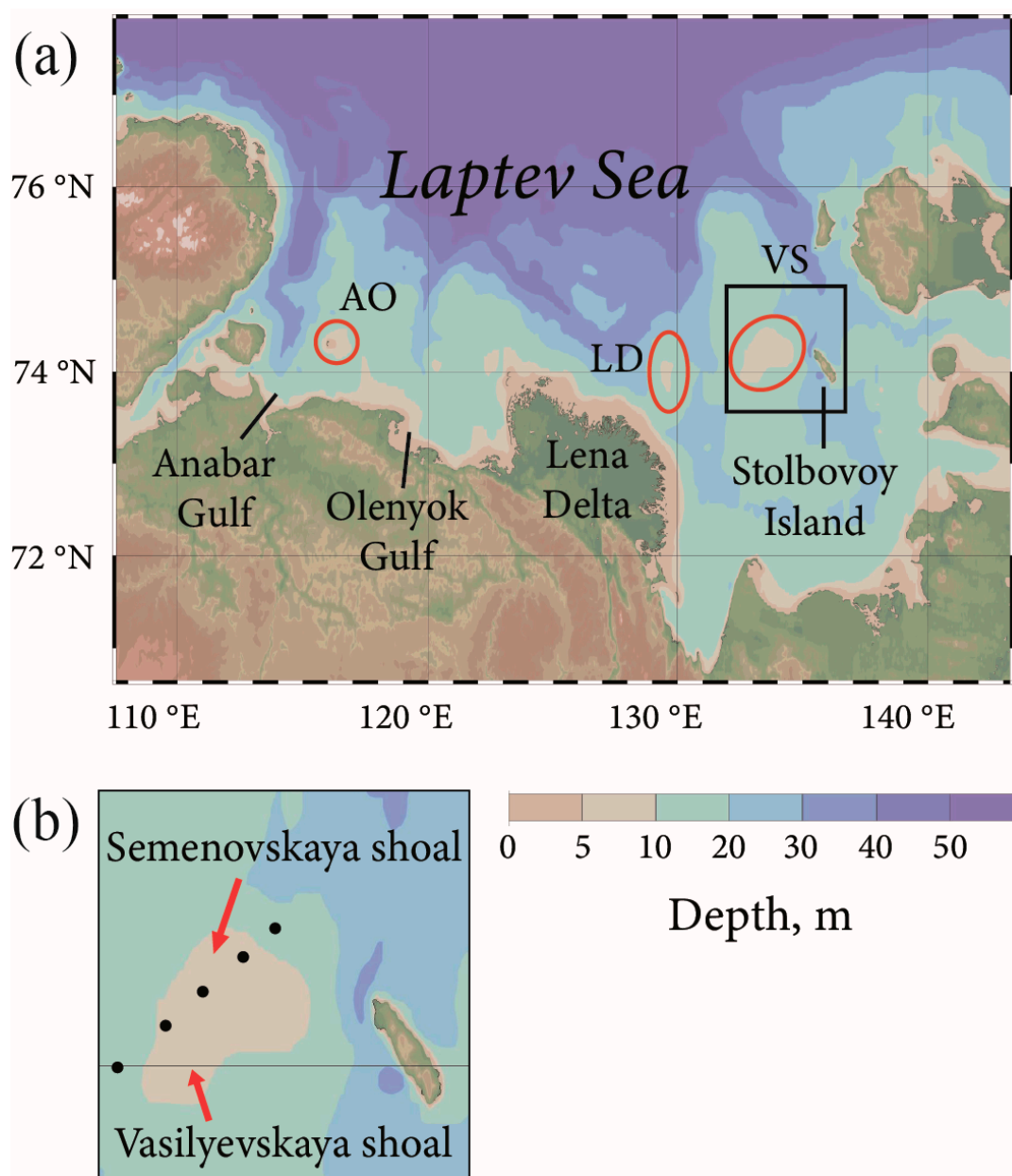

Figure 1. (**a**) Bathymetry of the Laptev Sea and location of the main shoals indicated by red ellipses. (**b**) Local bathymetry of the Vasilyevskaya and Semenovskaya shoals and location of the in situ measurements obtained in September 2005 (black dots) [48]. Black square in panel (**a**) indicates the zoomed-in area pictured in panel (**b**).

The most intense seafloor erosion occurs in the largest offshore shallow area of the Laptev Sea westward from the Stolbovoy Island, which consists of the closely located Vasilyevskaya and Semenovskaya shoals (hereafter referred to as VS) [41] (Figure 1b). Erosion of the submarine permafrost at this shoal is caused by wind- and wave-induced thermal abrasion of the submarine permafrost during ice-free periods and is enhanced by positive bottom layer temperatures [40]. This process manifests in increased turbidity in satellite images, which is not associated with the river discharge of coastal erosion due to the offshore location of these areas. Intense seafloor erosion is also registered by satellite observations at the shoal northeastward from the Anabar and Olenyok gulfs (hereafter referred to as AO), near the Lena Delta (hereafter referred to as LD) and at other smaller shallow regions at the Laptev Sea shelf (indicated by red ellipses in Figure 1).

Rapid thawing of the permafrost at all of these shoals due to increased bottom layer temperatures increases the entraining of suspended matter to seawater, which alters local sediment transport and depositions patterns [13]. This process significantly affects local topography and bathymetry, e.g., in the past it caused erosion and the disappearance of the Vasilyevskiy (in the 1930s) and Semenovskiy (in the 1960s) islands and the subsequent formation of Yaya Island (in the 2010s) at VS [13].

2.2. Satellite Data

This study is based on joint analysis of satellite imagery, wind and wave reanalysis, and in situ measurements. Satellite data consist of the MODIS Terra/Aqua optical imagery with a spatial resolution of 250 m and daily temporal coverage acquired in 2000–2021. In order to select relevant satellite data, all images acquired during the warm period (late June–early October) were visually inspected to avoid aliasing from sea ice and clouds. We did not use the available satellite products with a higher resolution (e.g., Sentinel-2/3, Landsat 7/8, MERIS). Despite the fact that they could provide better accuracy for studying turbid zones in the study area, they have less frequent temporal coverage, which is crucial for this work.

As was mentioned earlier, coastal erosion and river discharge are important sources of suspended sediment in the Laptev Sea, which form turbid zones along the coast and near river deltas and estuaries. Turbid zones formed by seafloor erosion, conversely, are localized at offshore sea areas that generally provide an opportunity to distinguish them from turbid zones associated with coastal erosion and river discharge. However, in many cases, seafloor erosion turbid zones coalesce with either coastal erosion zones or turbid river plumes. This process hinders accurate determination of the outer borders and areas of seafloor erosion turbid zones, which is among the main complexities of their study using satellite data.

The seafloor erosion area at VS, which is one of the largest in the Laptev Sea, is located far from the shoreline (Figure 1). This turbid area (even when it is fully developed) does not coalesce with coastal erosion zones or turbid river plumes. As a result, the outer border and area of seafloor erosion at VS could be clearly detected in satellite imagery. Conversely, another large seafloor erosion area at AO is located in close proximity to the shoreline (Figure 1) and is often overlapped with the coastal erosion turbidity zone. Similar to AO, the seafloor erosion zones at smaller shoals located near LD and in the southeastern part of the Laptev Sea (Figure 1) are often indistinguishable from turbid zones formed by river discharge and coastal erosion.

All available cloud-free and ice-free satellite images of VS, which is the main study region in the Laptev Sea (black rectangle in Figure 1), were numerically processed in order to distinguish the presence or absence of the erosion process and to reconstruct the area of the turbid zone in the latter case. For this purpose, the following ranges of RGB values corresponding to turbid zones in the processed images were determined: 30–50 for red, 30–60 for green, and 20–50 for blue. Once all three conditions were met by a pixel, it was marked as a part of a turbid zone, otherwise it was related to a nonturbid sea. The exact values of the area of the turbid zone (in km^2) reconstructed by this procedure were

used to qualitatively study the variability in the erosion intensity at VS in response to external forcing. In particular, we revealed the dependence of the reconstructed values on different days in 2000–2021 on synchronous wind-wave forcing conditions obtained from the numerical model, which is described below.

2.3. Wave Reanalysis Data

The wind-waves' parameters in the Laptev Sea were modeled by the WAVEWATCH III (WWIII) distributed by NOAA/NCEP [49]. This model allows the effect of wind forcing, ocean ice influence, wave energy dissipation, nonlinear interactions and bottom friction to be considered. The WWIII applies a numerical solution of the equation: $dN/dt = S/\sigma$, where $N(k, \theta) \equiv F(k, \theta)/\sigma$ is the wave action density, F is the energy density, k is the wavenumber, θ is the wave direction, σ is the relative frequency, d/dt is the total derivative and S is the total impact of sources and sinks [49]. S is the function that reproduces the wind energy transfer, nonlinear wave interactions, wave energy dissipation through the white capping and collapse in the shallow water, bottom friction, wave reflection and other processes. The WWIII output parameters are the following: significant wave height (SWH), wave propagation direction, mean wave period (WP) and mean wavelength (WL).

In this study, WWIII implementation with the ST6 scheme [50,51] was used. A Discrete Interaction Approximation (DIA) was used to reproduce nonlinear wave interactions. Sea ice coverage was considered by using the IC0 scheme, where a grid point is considered as ice-covered if ice concentration is >0.5. Bottom friction in the shallow water was considered by the JONSWAP scheme. The model was applied with 36 spectral directions and 36 frequency intervals (0.03–0.843 Hz) with the integration time step equal to 15 min.

As input data, the wind fields and ocean ice concentration data are received from the NCEP/CFSR reanalysis (1979–2010, spatial resolution ~0.3°) [52] and NCEP/CFSv2 reanalysis (2011–2021, spatial resolution ~0.2°) [53]; the time step of each reanalysis is 1 h (https://rda.ucar.edu accessed on 18 August 2023). The output time step was set as 3 h. The reanalysis data were linearly interpolated to a special unstructured mesh, which consists of 36,176 nodes (Figure 2). Linear interpolation of reanalysis data to the unstructured mesh was performed by using Python code. The interpolated wind fields were used in the wave model in mode "as is". The digital model of the bottom relief was obtained from the ETOPO 1 min database with the addition of digitized navigation maps. Navigation maps had a spatial resolution of about 500 m in the coastal zone. The mesh covers the Laptev, East Siberian, Chukchi and Beaufort seas (Figure 2). The mesh spatial resolution is ~800 m in the coastal zone and ~15 km in the northern parts of these seas. The computational grid has an open boundary at the north without any input data; however, these areas are covered by stable sea ice during the whole year. Open boundaries are also located at narrow straits in the west (Vilkitskiy Strait), east (M'Clure Strait and Amundsen Gulf) and south (Bering Strait), which significantly limits the wave energy flow (Figure 2). The WWIII model provides good quality results at low computational cost [54,55]. A comparison of the modeled and measured significant wave height by the mooring station in the Chukchi Sea provides the correlation coefficient equal to 0.94 and RMSE equal to 0.31 m [56]. Preliminary results based on this WWIII implementation, technical details and settings, and model quality assessments are presented in [56,57].
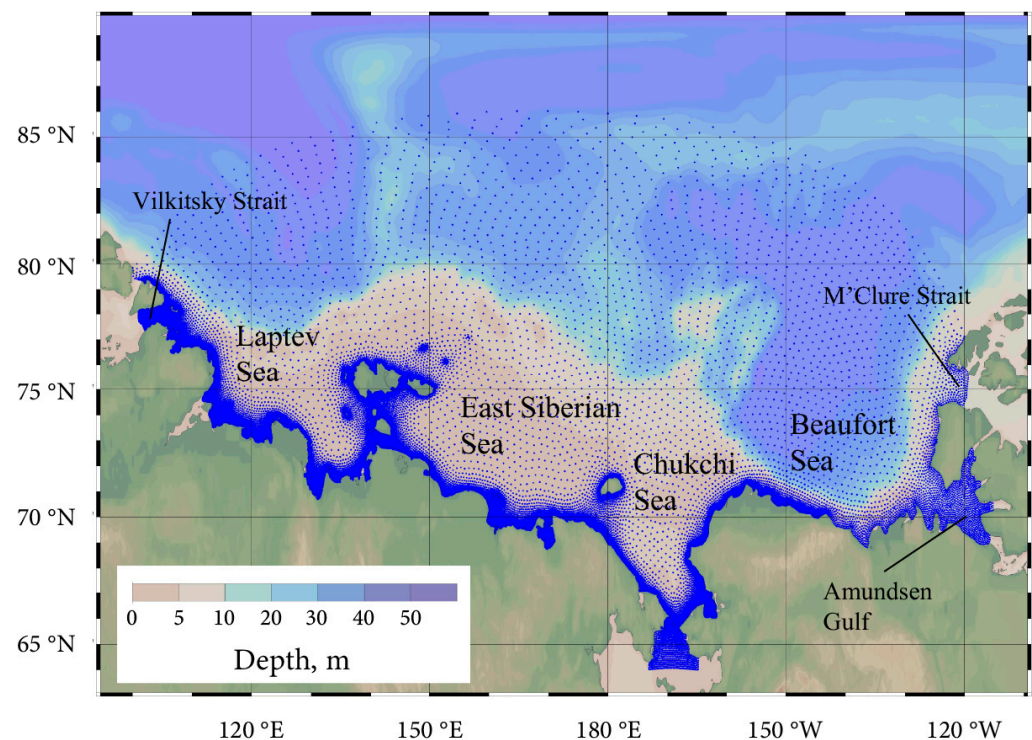
Figure 2. Unstructured mesh of the wave model for the Laptev, East Siberian, Chukchi and Beaufort seas.

3. Results

In this study, spatial and temporal variability in turbid seafloor erosion areas at VS, AO and smaller shoals near LD was analyzed. Then the isolated turbid zone at VS received special attention to study its response to the external forcing condition and to quantify fluxes of suspended sediments from this area. Similar procedures at other shoals were not performed as they were hindered due to their common coalescence with turbid zones formed by river discharge and coastal erosion.

3.1. Seafloor Erosion at VS

Seafloor erosion at VS was studied using 106 satellite images of the area. The majority of these images were acquired in August and September, while only 15 images correspond to July and October because of the almost constant presence of sea ice till late July and overcast conditions in October. The turbid zone at VS shows a high variability in shape, size and spatial position on the synoptic time scale caused by three main processes (Figure 3). During certain periods (with a duration from several days to several weeks), area of the turbid zone steadily increases, which indicates the continuous process of seafloor erosion. Figure 3a demonstrates an example of this process observed in late July and August 2011. Despite partial cloud coverage of the study area, it is clearly visible that the turbid zone increased by more than 10 times during 2.5 weeks from 29 July 2011 to 15 August 2011. Note that the growth intensity of the turbid region is not homogenous. The area of the turbid zone grows much slower during 29 July–8 August 2011 as compared to 8–15 August 2011. The satellite image of the study area acquired on 15 August 2011 demonstrates fully developed turbid regions at VS with a maximal area equal to 9300 km^2. The outer border of this area corresponds well with the isobath of 10 m (Figure 1b).
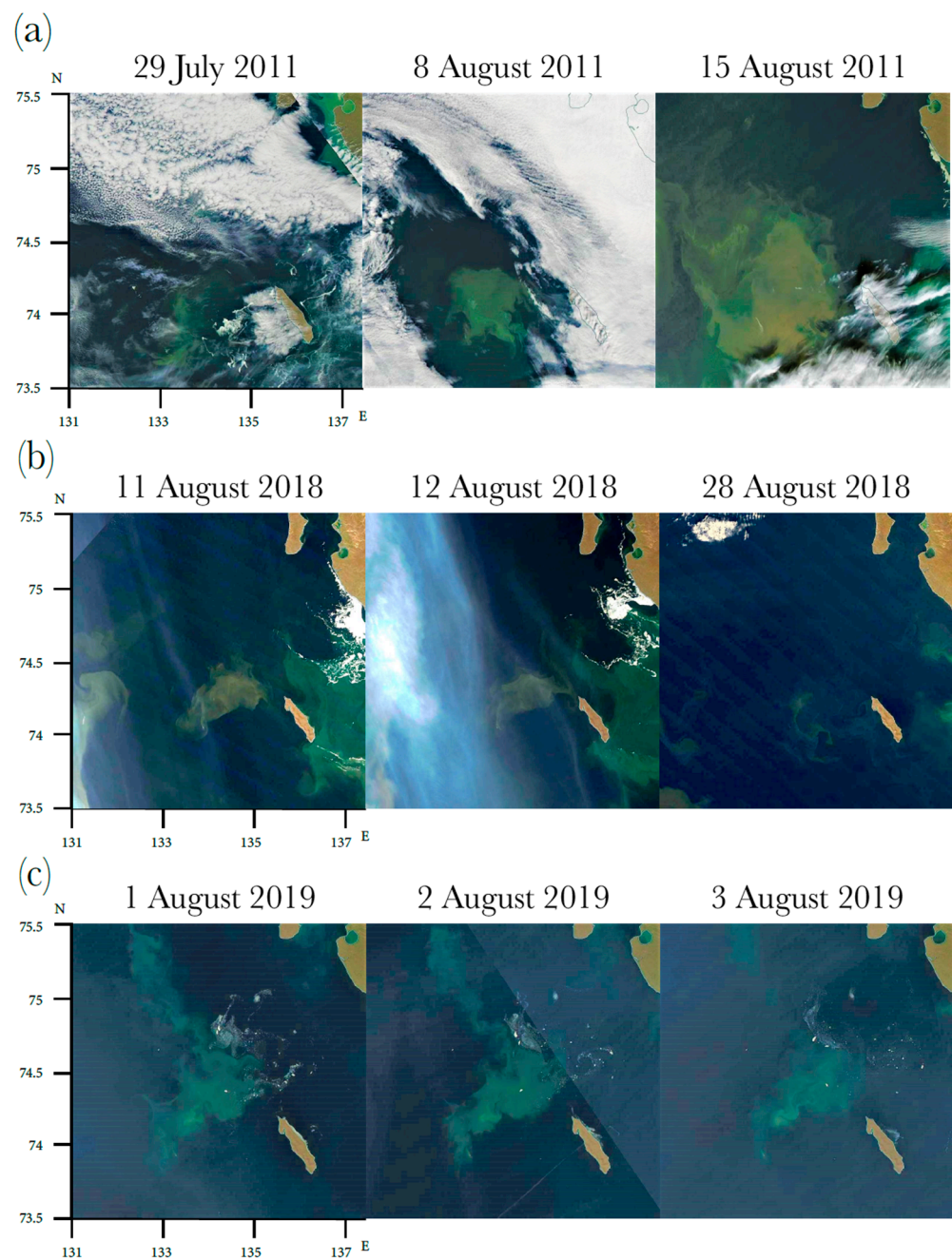
Figure 3. MODIS Terra/Aqua corrected reflectance images of VS illustrating (**a**) formation, (**b**) dissipation and (**c**) advection of local turbid area formed by seafloor erosion.

Dissipation of the turbid zone associated with the secession of seafloor erosion is also commonly observed in satellite images. This process is indicated by the steady decrease in the area of the turbid zone. Figure 3b demonstrates an example of dissipation registered in August 2018. The area of the turbid zone could significantly decrease during one day as was observed on 11–12 August 2018. On 28 August 2018, i.e., 16 days later, the area of the turbid zone at VS was <772 km^2, indicating its almost complete dissipation. Similar to formation periods, dissipation velocity was not homogenous for different observed periods. The third important process observed at VS is advection of the turbid zone, i.e., changes in its shape and position without significant changes in its area (Figure 3c). This process is associated with the horizontal motion of the turbid plume caused by intense shelf circulation without additional influx of eroded seafloor sediments. Based on the analyzed satellite images, the duration of the advection process is relatively short and does not exceed several days. The

typical time scale of the formation and dissipation of the turbid zone is much longer and is equal to 2–3 weeks. As a result, the advection process could be regarded as the early stage of the dissipation process.

3.2. Seafloor Erosion at AO and Small Shoals

Analysis of the spatial and temporal variability in the turbid zone associated with seafloor erosion at AO was hindered by its regular coalescence with the turbid zone associated with coastal erosion and river discharge (Figure 4). In the latter case, changes in the area, shape and size of the seafloor erosion zone were blurred by this coalescence (Figure 4b); therefore, only noncoalescence cases were considered (Figure 4a). As a result, only 38 satellite images of AO were analyzed.
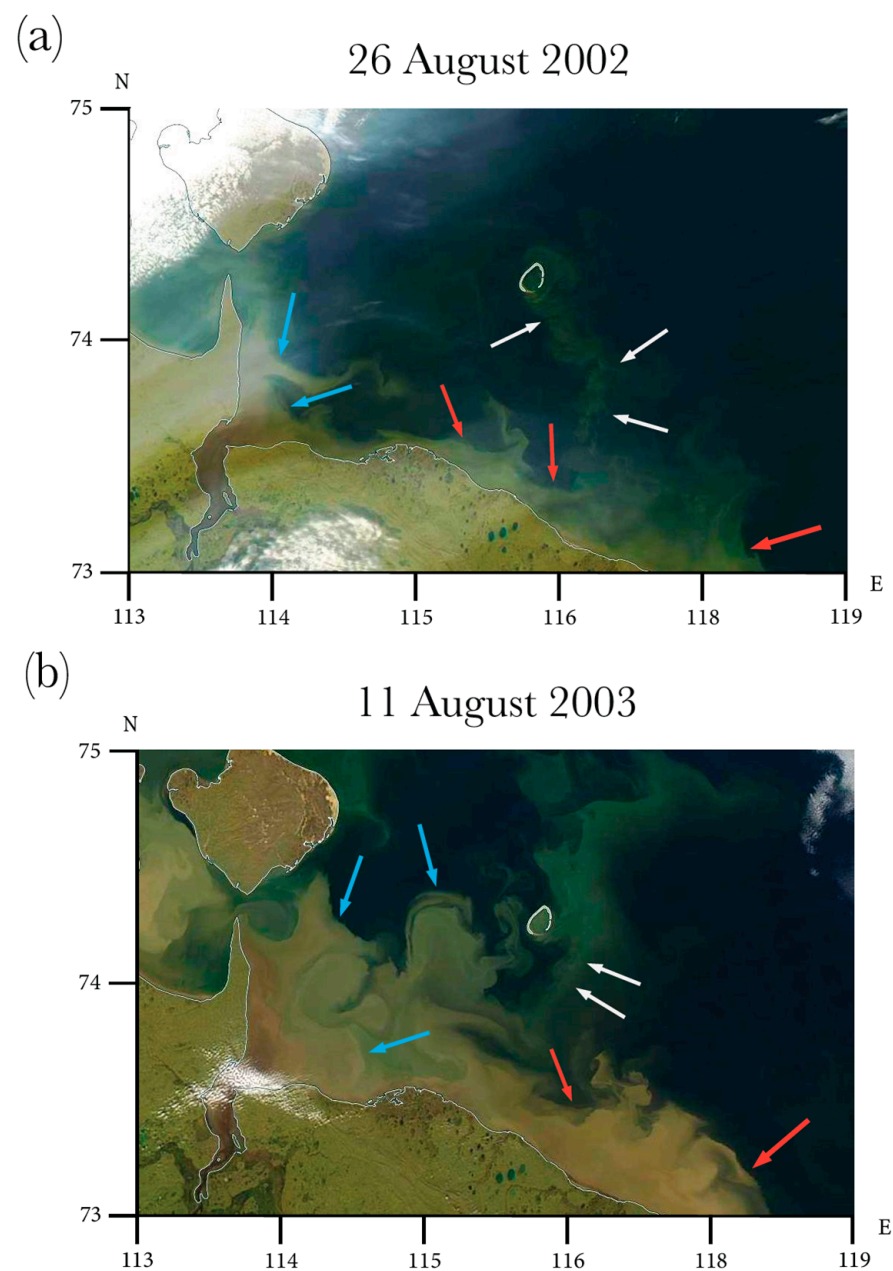

Figure 4. MODIS Terra/Aqua corrected reflectance images of AO illustrating (**a**) noncoalescence and (**b**) coalescence of turbid zones associated with seafloor erosion (white arrows), coastal erosion (red arrows) and river plumes (blue arrows).

As was previously carried out with VS, the formation, dissipation and advection processes of the turbid zone at AO were identified (Figure 5). Due to the smaller area of the shoal (~2 km^2) at AO as compared to that at VS (~6 km^2), which corresponds to the area of the well-developed seafloor erosion zone, the typical time scale of the formation and dissipation of the turbid zone at AO was equal to 6–10 days. Figure 5a demonstrates an example of the formation of the turbid zone at AO observed during 8–12 August 2011. Much as at VS, advection of the turbid zone at AO lasted for only 2–3 days (Figure 5b), which was further followed by its dissipation.
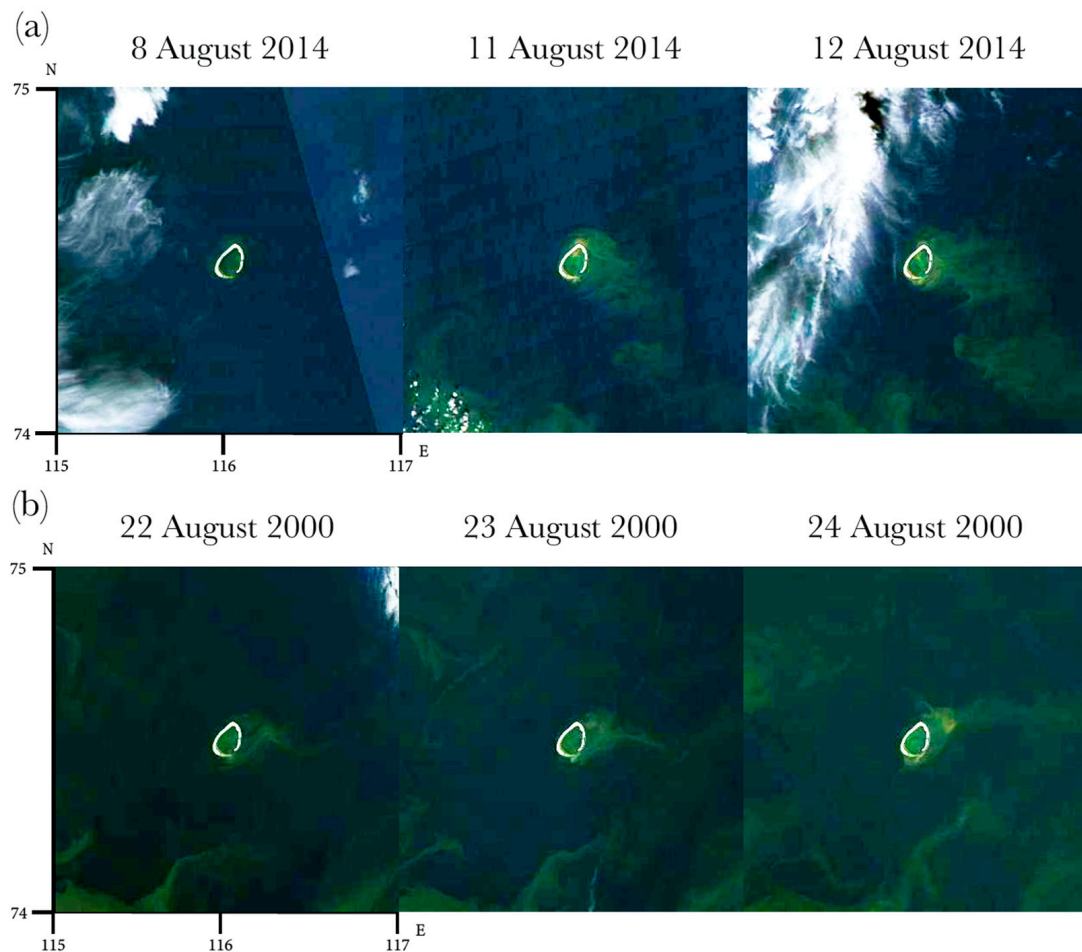

Figure 5. MODIS Terra/Aqua corrected reflectance images of AO illustrating (**a**) formation and (**b**) advection of local turbid area formed by seafloor erosion.

Apart from the two large shallow regions, VS and AO, seafloor erosion and the formation of the offshore turbid zones is also observed at a dozen small shoals in the Laptev Sea (Figure 6). Several shoals are located in the Olenyok Gulf (Figure 6a) and between the Olenyok Gulf and the Lena Delta close to Leykina Island (Figure 6b). Several more shoals are located northeastward (Figure 6b) and northwestward (Figure 6c) from the Lena Delta. Intense seafloor erosion at these areas is governed by wind-driven upwelling processes, which was described in [42]. The third group of shoals is located in the southeastern part of the Laptev Sea close to Zatoplyaemyy Island [13] (Figure 6d). The total area of all small offshore shoals in the Laptev Sea (except AO and VS) bounded by the isobaths of 10 m is estimated at ~2 km^2.

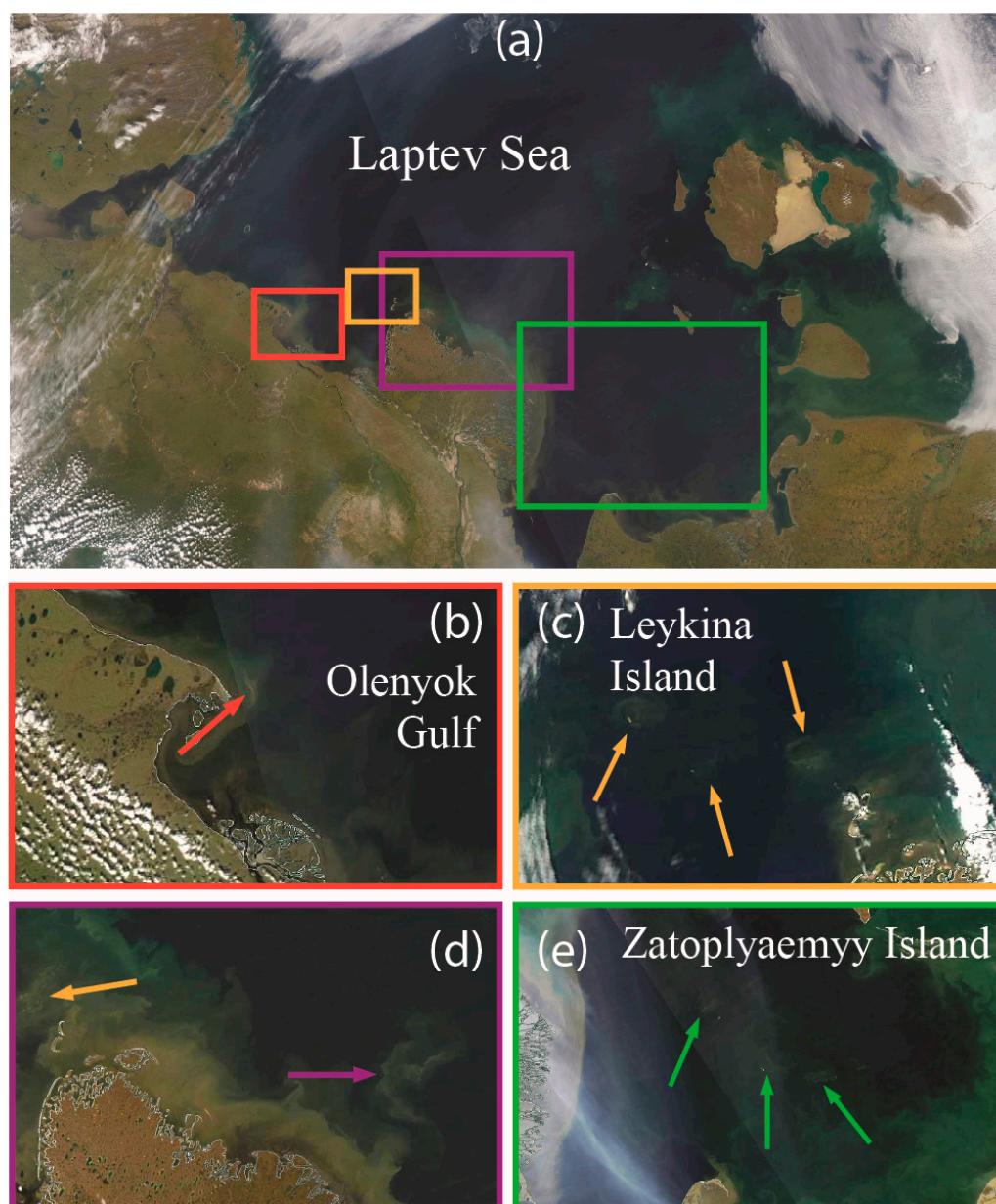**Figure 6.** MODIS Terra/Aqua satellite images of smaller shoals (indicated by arrows) (**a**) in the Laptev Sea, (**b**) in the Olenyok Gulf, (**c**) northwestward from the Lena Delta, (**d**) northeastward from the Lena Delta, (**e**) southeastward from the Lena Delta.

4. Discussion

Wind-induced waves have a direct effect on the area of the suspended sediment region. In shallow areas where wind-induced wave turbulence in the surface layer of the ocean is able to reach the seafloor, bottom sediment, eroded by the process of thermal abrasion, is entrained in the water column and rises to the surface layer appearing as a turbid region in the satellite images. Due to its distant location from coastal areas and relatively large size, we focused on the turbid zone at the VS study area to reveal its dependence on external forcing conditions, namely, wind and waves. For this purpose, the wind speed data obtained from NCEP/CFSR/CFSv2 reanalysis and wave length data were analyzed provided by the wave model described in Section 2.

The area of the turbid zone at VS for the 106 trial cases showed moderately strong linear dependence ($R > 0.6$) when associated with wave length values averaged for periods between 2 and 16 days. On the other hand, no relation was observed between the area

of the turbid zone at VS and both wind stress and wind speed. This reveals that wave length plays a predominant role in the formation of bottom resuspension at VS. The largest Pearson correlation coefficient R (0.74) between wave length (L in m) and an area of a turbid zone at VS (S in km^2) corresponds to the integration period of 9 days (Figure 7). The resulting regression equation that describes numerical dependence between the two variables is the following: S = 354·L − 7148.
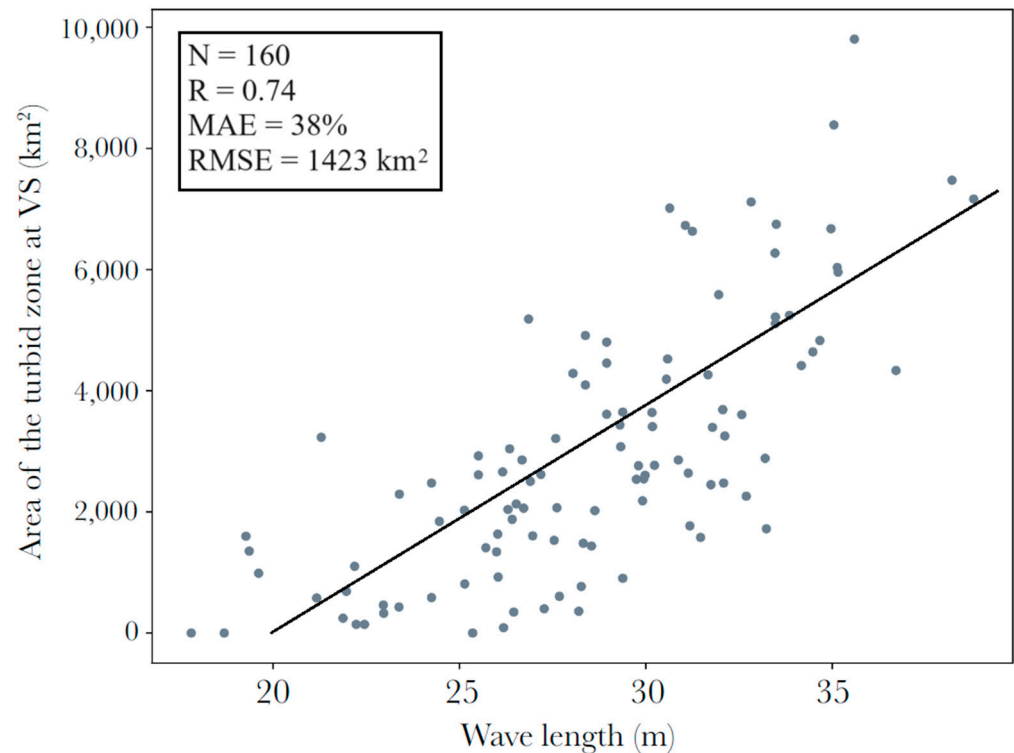

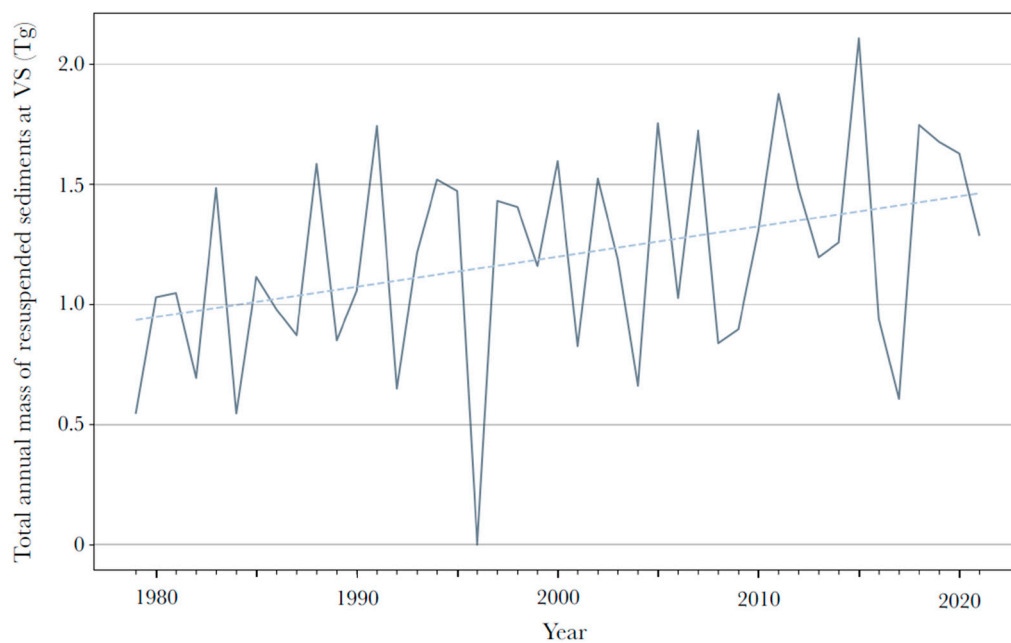**Figure 7.** Dependence between area of the turbid zone at VS and a 9-day average of wave length.

The mean absolute error of 38% quantifies the ability of this equation to reproduce absolute values of the area of the turbid zone at VS. The root mean square error is 1423 km^2 caused by the sensitivity of this characteristic to large errors. We note that the obtained regression showed better agreement with gauge measurements for low wave forcing cases compared to storm conditions. The obtained correlation coefficient R = 0.74 was also analysed using the Student's t-test. Using a confidence interval of 0.05 (α = 0.05, confidence level of 95%) and a number of degrees of freedom of 104 (v = n − 2) to determine the critical value of *t*, it was found that the absolute *t* value of the sample studied was greater than the critical value. Therefore, it can be concluded that the correlation present between wave length and the area of the turbid zone at VS is statistically significant.

The obtained regression equation described above was applied to obtain the daily areas of the turbid zone at VS during the ice-free season from 1979 to 2021 using wave reanalysis data calculated for this period. Note that in the case of the 9-day average of the wave length preceding a certain day being 20 m or less, the area of the turbid zone at VS at this day was presumed to be zero, i.e., the turbid zone was absent. The obtained area values were then used to calculate, first, the volume of seawater V, which contains the resuspended sediment at VS using bathymetry data from [48,58] and, second, the mass of the resuspended sediment M = V·C, where the average local concentration of the suspended sediment C = 15 mg/L was obtained from in situ measurements performed at VS in September 2005 (Figure 1b) [48]. The main statistical characteristics of the daily suspended sediment flux at VS during the ice-free season reconstructed for 1979–2021 are provided in Table 1.

Table 1. The main statistical characteristics of daily suspended sediment flux (in Tg) at VS during ice-free season reconstructed for 1979–2021.

Number of Cases	Mean	Median	Min	Max	Standard Deviation	Coefficient of Variation	Skewness
2948	0.33	0.31	0	1.05	0.17	53.22	0.53

In order to calculate the total annual mass of the resuspended sediment at VS, the resulting daily mass of the suspended sediment in the VS region was analysed and divided into separate events that corresponded to independent resuspension events. The mass change for each of these suspension events was calculated and summed to obtain a total resuspended mass per year. Figure 8 illustrates the inter-annual variability in the reconstructed total annual mass of the resuspended sediments at VS during the ice-free season in 1979–2021. The yearly total mass varies from 0.6 to 2.1 Tg with an average yearly value equal to 1.2 Tg. Considering the fact that, annually, the river discharge accounts for 24.1 Tg of sediment delivered to the Laptev Sea, while coastal abrasion provides 58.4 Tg [48], the resulting average annual sediment input by seafloor erosion at VS is only one order of magnitude smaller that the sediment flux by coastal erosion and riverine discharge.

Figure 8. Total annual flux of suspended sediments associated with seafloor erosion at VS during ice-free season in 1979–2021. The dashed line indicates an inter-annual trend. Note that no erosion occurred in 1996 because VS was covered by sea ice during the whole year.

Despite significant fluctuations, the overall trend for the analysed 43-year period is positive with the average annual flux increasing by 0.13 Tg every decade. This feature is caused by the increased length of the ice-free season (Figure 9a) in the Laptev Sea (reconstructed from satellite observations since 1979 [59]) and the resulting increase in the average wave length. The number of resuspension events during a year also shows a distinct increasing trend for the study period (Figure 9b). Seasonal variability in the resuspended sediment mass demonstrates low flux in July (0.1 Tg) and a significant increase in August–October (0.3–0.35 Tg) (Figure 10), which is also associated with local ice conditions. The largest monthly flux of resuspended sediments during the study period was registered in October 2015 and was equal to 0.68 Tg.
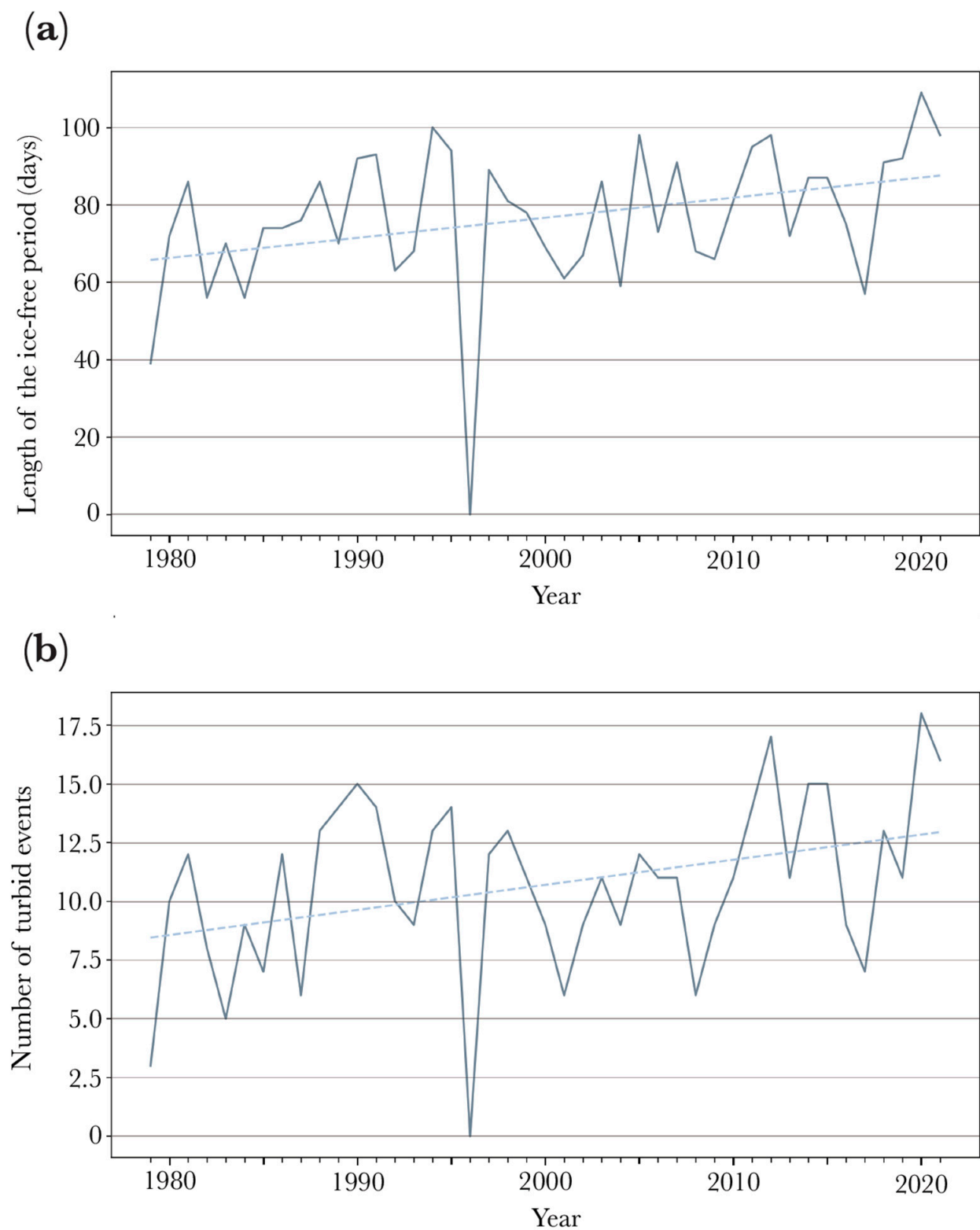
(a)

(b)

Figure 9. Duration of ice-free period (**a**) and number of resuspension events during ice-free season (**b**) at VS in 1979–2021. The dashed lines indicate inter-annual trends.
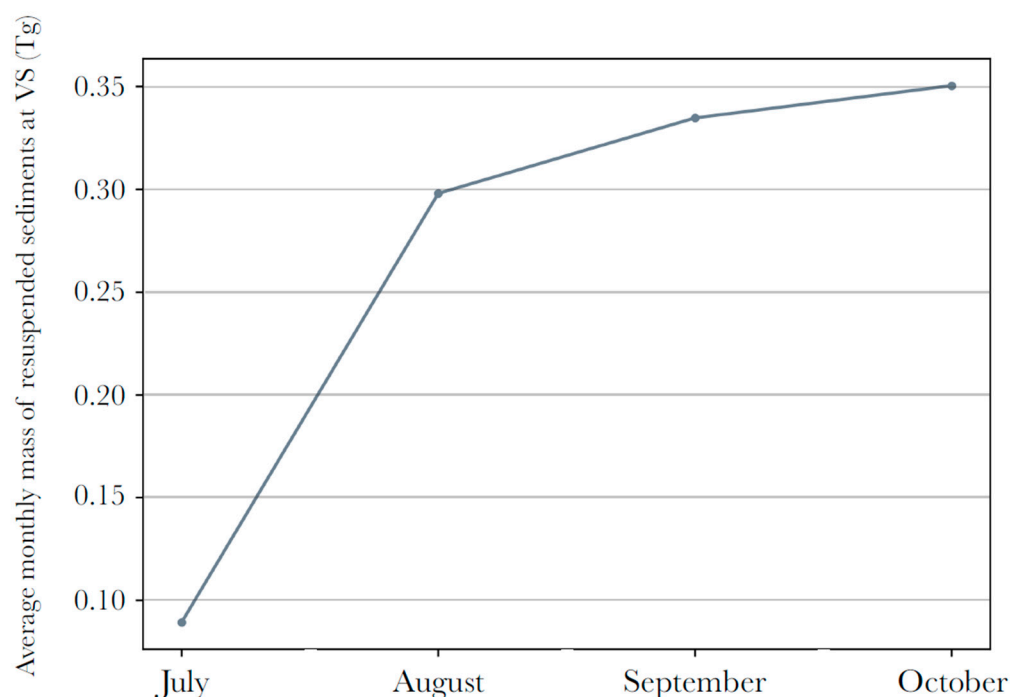
Figure 10. Average monthly flux of suspended sediments associated with seafloor erosion at VS in July–October in 1979–2021.

5. Conclusions

This study is focused on areas of seafloor erosion in the Laptev Sea that correspond to offshore shoals (with depths <10 m). Sediments resuspended from the seafloor penetrate upward towards the sea surface; as a result, seafloor erosion events at these shoals could be detected in cloud-free optical satellite imagery as turbid zones. Based on MODIS Terra/Aqua optical imagery acquired in 2000–2021, areas of frequent seafloor erosion at offshore shoals in the Laptev Sea were identified and synoptic variability in these turbid zones associated with their formation, dissipation and advection was described.

Sediment resuspension at the Vasilyevskaya and Semenovskaya shoals (VS), which are located in the southeastern part of the Laptev Sea, received special attention. Using wind and wave reanalysis data, it was revealed that sediment flux at VS under the first approximation is governed by wave forcing rather than wind stress. Intense resuspension of bottom sediments at VS is formed if the 9-day average of the wave length preceding the considered day exceeds 20 m. In this case, the area of the turbid zone (S, in km^2) formed at VS shows significant linear dependence (R = 0.74) on the local wave length (L, in m) averaged for the period of 9 days: S = 354·L − 7148.

Using this dependence, in situ measurements of the suspended sediment concentration in seawater at the study region and wave reanalysis data, daily volumes of sediment flux at VS during the ice-free season in 1979–2021 were assessed. The main limitation of this approach is the lack of data pertaining to sediment concentration variability. Moreover, we presume that the formation of the turbid region at VS manifests erosion of the submarine permafrost rather than the resuspension of previously accumulated sediments [60].

The reconstructed sediment input by seafloor erosion from VS (1.2 Tg per year on average) is 20–50 times smaller than those from two other major sources of sediment delivery in the Laptev Sea, namely, riverine discharge (24.1 Tg per year) and coastal abrasion (58.4 Tg per year). Inter-annual variability in the sediment flux at VS in 1979–2021 demonstrates a stable increasing trend (0.13 Tg every decade), which is caused by the increase in the length of the ice-free season in the study region. This feature demonstrates the increasing role of erosion of the subsea permafrost at shallow areas in the Laptev Sea caused by the ongoing climate change. Moreover, the total input from seafloor erosion

from all offshore shoals of the Laptev Sea could play a more significant role in the sediment income budget.

Finally, erosion of the subsea permafrost is important for local nutrient and carbon cycles [15,18,61]. The Laptev Sea and the entire East Siberian Arctic shelf could be employed as the integrator of the ongoing climate change in the surrounding environment. We suggest that under ongoing changes, more nutrients, the products of bottom and coastal eroded organic carbon transformation, as well as river runoff would be delivered to the Arctic Ocean with its shrinking ice cover potentially increasing primary production outside the shelf. At the same time, because the shelf area is characterized by very low transparency, which limits euphotic layer thickness, excessive pCO_2 would not be utilized by photosynthesis, but would rather be emitted to the atmosphere at increasing rates affecting the regional CO_2 balance. Thus, the proposed satellite technique could become an effective instrument to monitor and evaluate the increasing subsea permafrost erosion, which could be a potential and still uncounted contributor to the regional CO_2 system. The proposed methodology could also be applied to different coastal and shallow areas in the World Ocean, which experience intense delivery of terrigenous sediments, seafloor erosion and resuspension of sediments [62–65].

References

1. Stroeve, J.; Notz, D. Changing state of Arctic sea ice across all seasons. *Environ. Res. Lett.* **2018**, *13*, 103001. [CrossRef]
2. Box, J.E.; Colgan, W.T.; Christensen, T.R.; Schmidt, N.M.; Lund, M.; Parmentier, F.-J.W.; Brown, R.; Bhatt, U.S.; Euskirchen, E.S.; Romanovsky, V.E. Key indicators of Arctic climate change: 1971–2017. *Environ. Res. Lett.* **2019**, *14*, 045010. [CrossRef]
3. Lantuit, H.; Overduin, P.P.; Couture, N.; Wetterich, S.; Aré, F.; Atkinson, D.; Brown, J.; Cherkashov, G.; Drozdov, D.; Frobes, D.L.; et al. The Arctic coastal dynamics database: A new classification scheme and statistics on Arctic permafrost coastlines. *Estuaries Coasts* **2012**, *35*, 383–400. [CrossRef]
4. Fritz, M.; Vonk, J.E.; Lantuit, H. Collapsing Arctic coastlines. *Nat. Clim. Chang.* **2017**, *7*, 6–7. [CrossRef]
5. Ramage, J.L.; Irrgang, A.M.; Morgenstern, A.; Lantuit, H. Increasing coastal slump activity impacts the release of sediment and organic carbon into the Arctic Ocean. *Biogeosciences* **2018**, *15*, 1483–1495. [CrossRef]
6. Martens, J.; Romankevich, E.; Semiletov, I.; Wild, B.; van Dongen, B.; Vonk, J.; Tesi, T.; Shakhova, N.; Dudarev, O.V.; Kosmach, D.; et al. CASCADE—The Circum-Arctic Sediment CArbon DatabasE. *Earth Syst. Sci. Data* **2021**, *13*, 2561–2572. [CrossRef]
7. Shakhova, N.; Semiletov, I.; Gustafsson, O.; Sergienko, V.; Lobkovsky, L.; Dudarev, O.; Tumskoy, V.; Grigoriev, M.; Mazurov, A.; Salyuk, A.; et al. Current rates and mechanisms of subsea permafrost degradation in the East Siberian Arctic Shelf. *Nat. Commun.* **2017**, *8*, 15872. [CrossRef]
8. Angelopoulos, M.; Overduin, P.P.; Miesner, F.; Grigoriev, M.; Vasiliev, A. Recent advances in the study of Arctic submarine permafrost. *Permafr. Periglac. Process.* **2020**, *31*, 442–453. [CrossRef]

9. Paull, C.K.; Dallimore, S.R.; Jin, Y.K.; Melling, H. Rapid seafloor changes associated with the degradation of Arctic submarine permafrost. *Proc. Natl. Acad. Sci. USA* **2022**, *119*, e2119105119. [CrossRef]

10. Gavrilov, A.V.; Romanovskii, N.N.; Hubberten, H.-W.; Romanovskii, V.E. Distribution of islands—Ice complex remnants on the East Siberian arctic shelf. *Earth's Cryosphere* **2003**, *7*, 18–32.

11. Romanovskii, N.N.; Tumskoy, V.E. Retrospective approach to the estimation of the contemporary extension and structure of the shelf cryolithozone in east Arctic. *Earth's Cryosphere* **2011**, *15*, 3–14.

12. Overduin, P.P.; Wetterich, S.; Günther, F.; Grigoriev, M.N.; Grosse, G.; Schirmeister, L.; Hubberten, H.-W.; Makarov, A. Coastal dynamics and submarine permafrost in shallow water of the central Laptev Sea, East Siberia. *Cryopshere* **2016**, *10*, 1449–1462. [CrossRef]

13. Gavrilov, A.V.; Pizhankova, E.I. Dynamics of permafrost in the coastal zone of Eastern-Asian of the Arctic. *Geogr. Environ. Sustain.* **2018**, *11*, 20–37. [CrossRef]

14. Irrgang, A.M.; Bendixen, M.; Farquharson, L.M.; Baranskaya, A.V.; Erikson, L.H.; Gibbs, A.E.; Ogorodov, S.A.; Overduin, P.P.; Lantuit, H.; Grigoriev, M.N.; et al. Drivers, dynamics and impacts of changing Arctic coasts. *Nat. Rev. Earth Environ.* **2022**, *3*, 39–54. [CrossRef]

15. Vonk, J.; Sánchez-García, L.; van Dongen, B.E.; Alling, V.; Kosmach, D.; Charkin, A.; Semiletov, I.P.; Dudarev, O.V.; Shakhova, N.; Roos, P.; et al. Activation of old carbon by erosion of coastal and subsea permafrost in Arctic Siberia. *Nature* **2012**, *489*, 137–140. [CrossRef]

16. Wild, B.; Shakhova, N.; Dudarev, O.; Ruban, A.; Kosmach, D.; Tumskoy, V.; Tesi, T.; Grimm, H.; Nybom, I.; Matsubara, F.; et al. Organic matter composition and greenhouse gas production of thawing subsea permafrost in the Laptev Sea. *Nat. Commun.* **2022**, *13*, 5057. [CrossRef]

17. Semiletov, I.P. Destruction of frozen coastal rocks as an important factor in the biogeochemistry of Arctic shelf waters. *Dokl. Earth Sci.* **1999**, *368*, 679–682.

18. Semiletov, I.; Pipko, I.I.; Repina, I.A.; Shakhova, N. Carbonate dynamics and carbon dioxide fluxes across the atmosphere-ice-water interfaces in the Arctic Ocean Pacific sector of the Arctic. *J. Mar. Syst.* **2007**, *66*, 204–226. [CrossRef]

19. Semiletov, I.; Pipko, I.; Gustafsson, O.; Anderson, L.; Sergienko, V.; Pugach, S.; Dudarev, O.; Charkin, A.; Gukov, A.; Bröder, L.; et al. Acidification of East Siberian Arctic Shelf waters through addition of freshwater and terrestrial carbon. *Nat. Geosci.* **2016**, *9*, 361–365. [CrossRef]

20. Friedlingstein, P.; Cox, P.; Betts, R.; Bopp, L.; von Bloh, W.; Brovkin, V.; Cadule, P.; Doney, S.; Eby, M.; Fung, I.; et al. Climate–carbon cycle feedback analysis: Results from the C4MIP model intercomparison. *J. Clim.* **2006**, *19*, 3337–3353. [CrossRef]

21. Shakhova, N.; Semiletov, I.; Leifer, I.; Sergienko, V.; Salyuk, A.; Kosmach, D.; Chernikh, D.; Stubbs, C.; Nicolsky, D.; Tumskoy, V.; et al. Ebullition and storm-induced methane release from the East Siberian Arctic Shelf. *Nat. Geosci.* **2014**, *7*, 64–70. [CrossRef]

22. Vetrov, A.A.; Romankevich, E.A. *Carbon Cycle in the Russian Arctic Seas*; Springer: Berlin, Germany, 2004.

23. Charkin, A.V.; Dudarev, O.V.; Semiletov, I.P.; Kruhmalev, A.V.; Vonk, J.E.; Sánchez-García, L.; Karlsson, E.; Gustafsson, Ö. Seasonal and interannual variability of sedimentation and organic matter distribution in the Buor-Khaya Gulf: The primary recipient of input from Lena River and coastal erosion in the southeast Laptev Sea. *Biogeosciences* **2011**, *8*, 2581–2594. [CrossRef]

24. Semiletov, I.P.; Pipko, I.I.; Shakhova, N.E.; Dudarev, O.V.; Pugach, S.P.; Charkin, A.N.; McRoy, C.P.; Kosmach, D.; Gustafsson, Ö. Carbon transport by the Lena River from its headwaters to the Arctic Ocean, with emphasis on fluvial input of terrestrial particulate organic carbon vs. carbon transport by coastal erosion. *Biogeosciences* **2011**, *8*, 2407–2426. [CrossRef]

25. Wegner, S.; Hölemann, J.A.; Dmitrenko, I.; Kirillov, S.; Tuschling, K.; Abramova, E.; Kassens, H. Suspended particulate matter on the Laptev Sea shelf (Siberian Arctic) during ice-free conditions. *Estuar. Coast. Shelf Sci.* **2003**, *57*, 55–64. [CrossRef]

26. Wegner, S.; Hölemann, J.A.; Dmitrenko, I.; Kirillov, S.; Kassens, H. Seasonal variations in Arctic sediment dynamics—Evidence from 1-year records in the Laptev Sea (Siberian Arctic). *Glob. Planet. Chang.* **2005**, *48*, 126–140. [CrossRef]

27. Wegner, S.; Bauch, D.; Hölemann, J.A.; Janout, M.A.; Heim, B.; Novikhin, A.; Kassens, H.; Timokhov, L. Interannual variability of surface and bottom sediment transport on the Laptev Sea shelf during summer. *Biogeosciences* **2013**, *10*, 1117–1129. [CrossRef]

28. Drits, A.V.; Pasternak, A.F.; Arashkevich, E.G.; Kravchishina, M.D.; Sukhanova, I.N.; Sergeeva, V.M.; Flirt, M.V. Influence of riverine discharge and timing of ice retreat on particle sedimentation patterns on the Laptev Sea shelf. *J. Geophys. Res. Ocean.* **2021**, *126*, e2021JC017462. [CrossRef]

29. Osadchiev, A.; Medvedev, I.; Shchuka, S.; Kulikov, M.; Spivak, E.; Pisareva, M.; Semiletov, I. Influence of estuarine tidal mixing on structure and spatial scales of large river plumes. *Ocean Sci.* **2020**, *16*, 781–798. [CrossRef]

30. Osadchiev, A.; Frey, D.; Spivak, E.; Shchuka, S.; Tilinina, N.; Semiletov, I. Structure and inter-annual variability of the freshened surface layer in the Laptev and East-Siberian seas during ice-free periods. *Front. Mar. Sci.* **2021**, *8*, 735011. [CrossRef]

31. Osadchiev, A. Spreading and transformation of river discharge in the Arctic Ocean. *Her. Russ. Acad. Sci.* **2021**, *91*, 694–699. [CrossRef]

32. Spivak, E.A.; Osadchiev, A.A.; Semiletov, I.P. Structure and variability of the Lena River plume in the south-eastern part of the Laptev Sea. *Oceanology* **2021**, *61*, 839–849. [CrossRef]

33. Xie, L.; Yakushev, E.V.; Semiletov, I.; Grinko, A.; Gangnus, I.; Berezina, A.; Osadchiev, A.; Zhdanov, I.; Polukhin, A.; Moiseeva, J.; et al. Biogeochemical structure of the Laptev Sea in 2015, 2017-2020 associated with the river Lena plume. *Front. Mar. Sci.* **2023**, *10*, 1180054. [CrossRef]

34. Eicken, H.; Reimnitz, E.; Alexadrov, V.; Martin, T.; Kassens, H.; Viehoff, T. Sea-ice processes in the Laptev Sea and their importance for sediment export. *Cont. Shelf Res.* **1997**, *17*, 205–233. [CrossRef]

35. Dethleff, D. Entrainment and export of Laptev Sea ice sediments, Siberian Arctic. *J. Geophys. Res. Ocean.* **2005**, *110*, C07009.

36. Wegner, C.; Wittbrodt, K.; Hölemann, J.A.; Janout, M.A.; Krumpen, T.; Selyuzhenok, V.; Novikhin, A.; Polyakova, Y.; Krykova, I.; Kassens, H. Sediment entrainment into sea ice and transport in the Transpolar Drift: A case study from the Laptev Sea in winter 2011/2012. *Cont. Shelf Res.* **2017**, *141*, 1–10. [CrossRef]

37. Clarke, T.L.; Lesht, B.; Young, R.A.; Swift, D.J.P.; Freeland, G.L. Sediment resuspension by surface-wave action: An examination of possible mechanisms. *Mar. Geol.* **1982**, *49*, 43–59. [CrossRef]

38. Kularatne, S.; Pattiaratchi, C. Turbulent kinetic energy and sediment resuspension due to wave groups. *Cont. Shelf Res.* **2008**, *28*, 726–736. [CrossRef]

39. Carlin, J.A.; Lee, G.-h.; Dellapenna, T.M.; Laverty, P. Sediment resuspension by wind, waves, and currents during meteorological frontal passages in a micro-tidal lagoon. *Estuar. Coast. Shelf Sci.* **2016**, *172*, 24–33. [CrossRef]

40. Dmitrenko, I.A.; Hölemann, J.; Kirillov, S.A.; Berezovskaya, S.L.; Kassens, H. Role of barotropic sealevel changes in current formation on the eastern shelf of the Laptev Sea. *Dokl. Earth Sci.* **2001**, *5*, 243–249.

41. Juhls, B.; Overduin, P.P.; Hölemann, J.; Hieronymi, M.; Matsuoka, A.; Heim, B.; Fischer, J. Dissolved organic matter at the fluvial–marine transition in the Laptev Sea using in situ data and ocean colour remote sensing. *Biogeosciences* **2019**, *16*, 2693–2713. [CrossRef]

42. Osadchiev, A.; Silvestrova, K.; Myslenkov, S. Wind-driven coastal upwelling near large river deltas in the Laptev and East-Siberian seas. *Remote Sens.* **2020**, *12*, 844. [CrossRef]

43. Pavlov, V.K.; Timokhov, L.A.; Baskakov, G.A.; Kulakov, M.Y.; Kurazhov, V.K.; Pavlov, P.V.; Pivovarov, S.V.; Stanovoy, V.V. *Hydrometeorological Regime of the Kara, Laptev, and East-Siberian Seas*; Technical Memorandum, APL-UW TM 1-96; Defense Technical Information Center: Fort Belvoir, VA, USA, 1996.

44. Chuvilin, E.; Bukhanov, B.; Yurchenko, A.; Davletshina, D.; Shakhova, N.; Spivak, E.; Rusakov, V.; Dudarev, O.; Khaustova, N.; Tikhonova, A.; et al. In-situ temperatures and thermal properties of the East Siberian Arctic shelf sediments: Key input for understanding the dynamics of subsea permafrost. *Mar. Pet. Geol.* **2022**, *138*, 105550. [CrossRef]

45. Bukhanov, B.; Chuvilin, E.; Zhmaev, M.; Shakhova, N.; Spivak, E.; Dudarev, O.; Osadchiev, A.; Spasennykh, M.; Semiletov, I. In situ bottom sediment temperatures in the Siberian arctic seas: Current state of subsea permafrost in the Kara Sea vs Laptev and East Siberian seas. *Mar. Pet. Geol.* **2023**, *157*, 106467. [CrossRef]

46. Koshurnikov, A.V.; Tumskoy, V.E.; Shakhova, N.E.; Sergienko, V.I.; Dudarev, O.V.; Gunar, A.Y.; Pushkarev, P.Y.; Semiletov, I.P. The first ever application of electromagnetic soundings for mapping of submarine permafrost table on the Laptev Sea shelf. *Dokl. Earth Sci.* **2016**, *469*, 860–863. [CrossRef]

47. Alekseev, D.A.; Koshurnikov, A.V.; Gunar, A.Y.; Balikhin, E.I.; Semiletov, I.P.; Shakhova, N.E.; Palshin, N.A.; Lobkovsky, L.I. Time-domain electromagnetics for subsea permafrost mapping in the Arctic: The synthetic response analyses and uncertainty estimates from numerical modelling data. *Geosciences* **2023**, *13*, 144. [CrossRef]

48. Dudarev, O.V.; Charkin, A.N.; Shakhova, N.E.; Semiletov, I.P.; Sergienko, V.I.; Pipko, I.I.; Pugach, S.P.; Chernykh, D.V. Features of modern morpholithogenesis on the shelf of the Laptev Sea: Semenovskoe shoal ("Vasema Land"). *Dokl. Erath Sci.* **2015**, *462*, 223–229.

49. Tolman, H.L. *User Manual and System Documentation of WAVEWATCH III TM Version 3.14*; Technical note, MMAB Contribution; National Oceanic and Atmospheric Administration: Washington, DC, USA, 2009.

50. Rogers, W.E.; Babanin, A.V.; Wang, D.W. Observation-consistent input and whitecapping dissipation in a model for wind-generated surface waves: Description and simple calculations. *J. Atmos. Ocean. Technol.* **2012**, *29*, 1329–1346. [CrossRef]

51. Zieger, S.; Babanin, A.V.; Rogers, W.E.; Young, I.R. Observation-based source terms in the third-generation wave model WAVEWATCH. *Ocean Model.* **2015**, *96*, 2–25. [CrossRef]

52. Saha, S.; Moorthi, S.; Pan, H.L.; Wu, X.; Wang, J.; Nadiga, S.; Goldberg, M. The NCEP climate forecast system reanalysis. *Bull. Am. Meteorol. Soc.* **2010**, *91*, 1015–1057. [CrossRef]

53. Saha, S.; Moorthi, S.; Wu, X.; Wang, J.; Nadiga, S.; Tripp, P.; Becker, E. The NCEP climate forecast system Version 2. *J. Clim.* **2014**, *27*, 2185–2208. [CrossRef]

54. Liu, Q.; Rogers, W.E.; Babanin, A.V.; Young, I.R.; Romero, L.; Zieger, S.; Qiao, F.; Guan, C. Observation-based source terms in the third-generation wave model WAVEWATCH III: Updates and verification. *J. Phys. Oceanogr.* **2019**, *49*, 489–517. [CrossRef]

55. Myslenkov, S.; Kruglova, E.; Medvedeva, A.; Silvestrova, K.; Arkhipkin, V.; Akpinar, A.; Dobrolyubov, S. Number of storms in several Russian seas: Trends and connection to large-scale atmospheric indices. *Russ. J. Earth Sci.* **2023**, *23*, ES3002. [CrossRef]

56. Myslenkov, S.A. Modeling of the wind waves in the Laptev, East Siberian and Chukchi seas. *Hydrometeorol. Res. Forecast.* **2023**, *1*, 87–101. [CrossRef]

57. Myslenkov, S.A.; Platonov, V.S.; Dobrolyubov, S.A.; Silvestrova, K.P. Increase in storm activity in the Kara Sea from 1979 to 2019: Numerical simulation data. *Dokl. Earth Sci.* **2021**, *498*, 502–508. [CrossRef]

58. Jakobsson, M.; Mayer, L.A.; Coakley, B.; Dowdeswell, J.A.; Forbes, S.; Fridman, B.; Hodnesdal, H.; Noormets, R.; Pedersen, R.; Rebesco, M.; et al. The international bathymetric chart of the Arctic Ocean (IBCAO), Version 3.0. *Geophys. Res. Lett.* **2012**, *39*, L12609. [CrossRef]

59. Cavalieri, D.J.; Parkinson, C.L. Arctic sea ice variability and trends, 1979–2010. *Cryosphere* **2012**, *6*, 881–889. [CrossRef]

60. Rachold, V.; Grigoriev, M.N.; Are, F.E.; Solomon, S.; Reimnitz, E.; Kassens, H.; Antonow, M. Coastal erosion vs riverine sediment discharge in the Arctic Shelf seas. *Int. J. Earth Sci.* **2000**, *89*, 450–460. [CrossRef]

61. Sukhanova, I.N.; Flirt, M.V.; Georgieva, E.J.; Lange, E.K.; Kravchishina, M.D.; Demidov, A.B.; Nedospasov, A.A.; Polukhin, A.A. The structure of phytoplankton communities in the eastern part of the Laptev Sea. *Oceanology* **2017**, *57*, 75–90. [CrossRef]

62. Korotkina, O.A.; Zavialov, P.O.; Osadchiev, A.A. Submesoscale variability of the current and wind fields in the coastal region of Sochi. *Oceanology* **2011**, *51*, 745–754. [CrossRef]

63. Korotkina, O.A.; Zavialov, P.O.; Osadchiev, A.A. Synoptic variability of currents in the coastal waters of Sochi. *Oceanology* **2014**, *54*, 545–556. [CrossRef]

64. Korotenko, K.A.; Osadchiev, A.A.; Zavialov, P.O.; Kao, R.-C.; Ding, C.-F. Effects of bottom topography on dynamics of river discharges in tidal regions: Case study of twin plumes in Taiwan Strait. *Ocean Sci.* **2014**, *10*, 865–879. [CrossRef]

65. Osadchiev, A.A.; Korotenko, K.A.; Zavialov, P.O.; Chiang, W.-S.; Liu, C.-C. Transport and bottom accumulation of fine river sediments under typhoon conditions and associated submarine landslides: Case study of the Peinan River, Taiwan. *Nat. Hazards Earth Syst. Sci.* **2016**, *16*, 41–54. [CrossRef]